Application of statistical functions for microstructure characterization and determination of elastic properties of ceramic foam

Vinit Vijay Deshpande[1], Romana Piat[1] and Kay André Weidenmann[2]

[1] Department of Mathematics and Natural Sciences, University of Applied Sciences Darmstadt, Schöfferstraße 3, Darmstadt 64295, Germany
[2] Institute of Materials Resource Management (MRM), University of Augsburg, Universitätsstraße 1, Augsburg 86159, Germany

vinit-vijay.deshpande@h-da.de,romana.piat@h-da.de,
kay.weidenmann@mrm.uni-augsburg.de

Abstract. Microstructural features of ceramic foam are numerically evaluated by employing statistical functions. X-ray computed tomography (CT) scans of ceramic foam are utilized to compute statistical functions like two-point correlation function, lineal path function, etc. These functions describe the microstructure of the foam. Segmentation algorithms are applied to isolate the voids and study their shape distribution within the sample. The statistical functions are further utilized to determine the correct size of the stochastic volume elements (SVEs) that can represent the entire foam sample. Ensemble averaging and size enlargement effects on different SVE sizes are evaluated. By comparing the statistical functions of the entire sample with that of the ensemble of correctly sized SVEs, a ranking method is developed to determine the SVE positions inside the sample that resemble the most with the entire sample. These SVEs are then adopted to determine the effective elastic properties of the foam sample. Finite element models of the selected SVEs are constructed and mixed uniform boundary conditions are applied to numerically determine the coefficients of effective stiffness tensor. Lastly, the obtained properties are compared with experimental results available in the literature.

Keywords: Ceramic foam, elastic properties, microstructure characterization, statistical functions, numerical modelling, X-ray computed tomography

1 Introduction

Nowadays, composite materials are extensively used in a variety of industries including but not limited to aerospace, automotive, medical devices, oil and gas, electronics, etc. Generally, a composite material consists of discontinuous reinforcement phase distributed within a continuous medium called matrix [1]. This reinforcement phase can be particles of various shapes and sizes, fibers or whiskers. An exception to this definition

is a type of composite called interpenetrating phase composite. In these composites, both the phases are continuous and hence cannot be differentiated into matrix and reinforcement. These composites are especially beneficial when there is a need for a material to possess contradictory properties [2]. Their manufacturing involves producing an open porous preform which is then infiltrated by for example a molten metal [3]. The manufacturing method and microstructure of this preform are highly important parameters as they govern the final distribution of phases in the composite.

In this work, an alumina preform manufactured via a slurry base route [3] is studied numerically with an objective to quantify its microstructural features and to use them in determining its effective elastic properties. The preform microstructure is highly porous with voids resembling spheres that are connected to each other, hence the name 'foam'. These voids are characterized by isolating them using image processing algorithms. They are then studied to check their resemblance to spheres and their orientation distribution within the sample space.

Torquato el al [4, 5] has given detailed description of various statistical functions that are used to describe the microstructure of heterogeneous materials. These functions are n-point correlation functions each uniquely describing the distribution of phases inside the material. They are used in the present work to describe the distribution of porosity within the foam sample. They are calculated for the entire sample and are used to derive important observations on material symmetry and homogeneity of the sample.

In order to evaluate the effective elastic properties of the foam, it is important to determine the appropriate size of a volume element (VE) within the sample that can act as a stochastic volume element (SVE). Statistical functions are used to determine this size by dividing the foam sample into smaller volume elements of different sizes. These functions are then calculated for each VE of each size and the size effects are studied in terms of ensemble averaging and sample enlargement. This study results in determination of a VE size that can act as SVE to the foam sample.

Ensemble average of the effective elastic properties of this SVE can give a good estimate of the effective properties of the entire sample in question. But this will lead to considerable computational expenses as number of VE realizations for selected SVE size would be large. To reduce this number, a ranking method is developed in which VEs are ranked based upon how close their statistical functions are to that of the entire sample. Based upon this, a relatively small number of VEs are selected for averaging.

Finite element methods are predominantly used to solve structural mechanics problems numerically. These methods involve discretizing the continuous media into smaller defined shapes called elements within which field variables (stress, strain, displacement, etc) are interpolated using shape functions. They are widely used for evaluating effective material properties of heterogeneous media. The ensemble of VEs selected from the ranking method are meshed and mixed uniform boundary conditions [6] are applied to determine effective linear elastic stiffness coefficients of each VE. Following ensemble averaging, we get effective properties of the entire foam sample.

Lastly, the procedure described above is validated by comparing the calculated effective properties with experimental measurements [3]. The comparison shows that statistical functions can be used to define appropriate size of SVEs and the ranking method helps to reduce the computational effort which would have otherwise required.

The article is organized into following sections: Section 2 describes the image processing steps performed on microcomputed tomography (μCT) scans of the foam sample, segmentation of pores and their shape distribution within the sample. Section 3 includes definition of statistical functions and their evaluation for the entire sample. Section 4 describes the procedure to select appropriate size of SVE. Section 5 describes the ranking procedure. Section 6 describes finite element calculations to determine effective elastic properties followed by comparison with experimental results. The discussion on the entire procedure is in section 7 followed by conclusions in section 8.

2 Image Processing of μCT Data

A cubic sample of dimensions $V \approx 5 \times 5 \times 5$ mm^3 was scanned using X-ray computed tomography. To avoid artifacts like beam hardening on the boundaries of the cube, a smaller region in the interior of the sample with dimensions $V_i \approx 1.89 \times 1.76 \times 1.94$ mm^3 was selected. Details regarding the image processing can be found in [3]. The μCT data is available in the form of 2D cross sections of the foam sample with each cross section being a grayscale image. These images are stacked one on top of other to form a 3D volumetric map. This is followed by removal of any noise by using median filter. Next, a global threshold in terms of a scalar luminance value is determined which is used to binarize the 3D image. This is done iteratively by altering the threshold value such that after binarization, the final porosity obtained by counting pore voxels matches that obtained by experimental measurements. The porosity of the foam sample obtained by density measurements was 74.5% [3]. Hence the global threshold value is decided such that the porosity in binarized 3D image matches this value. After binarization, a 3D image with pore regions marked as '0' (black color) and alumina region marked as '1' (white color) is obtained. Lastly, an area opening operation is performed in which all the connected regions of alumina phase having volume less than 10 voxels are removed. This removes any hovering alumina regions lying within the pore phase (Fig. 1a).

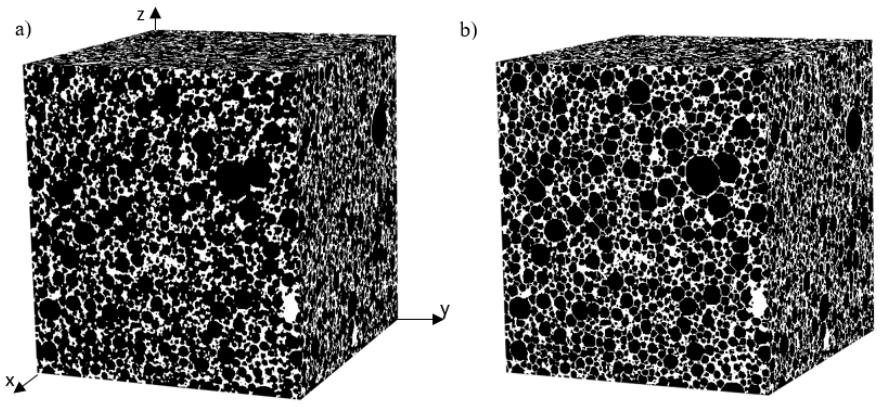

Fig. 1. a) Binarized 3D image before segmentation and b) after segmentation

It can be seen from Fig.1a that the pores are interconnected to each other. In order to isolate them, a segmentation method called watershed algorithm [7] is applied. The resulting image is shown in Fig.1b. Thereafter, the individual pores are studied separately to calculate their volume, surface area and orientation. Sphericity of each pore is also calculated which quantifies how close the shape of the pore is with respect to a sphere. It is defined as the ratio of surface area of an equal-volume sphere to the actual surface area of the pore [8]. Its expression is given as:

$$\psi = \frac{\pi^{1/3}\,(6V_p)^{2/3}}{A_p}. \tag{1}$$

Here, V_p is volume of pore and A_p is surface area of pore. Fig. 2a shows cumulative distribution of pore sphericity with pore volume fraction. Pore volume fraction is defined as volume fraction of a particular pore with respect to all the pores present in the sample. Note that the pores that lie at the boundary of the foam sample are not considered in this study because of lack of information about the entire pore. It can be seen that all the pores have sphericity greater than 0.75 and 90% of the pores have sphericity greater than 0.86. The maximum sphericity is 0.97.

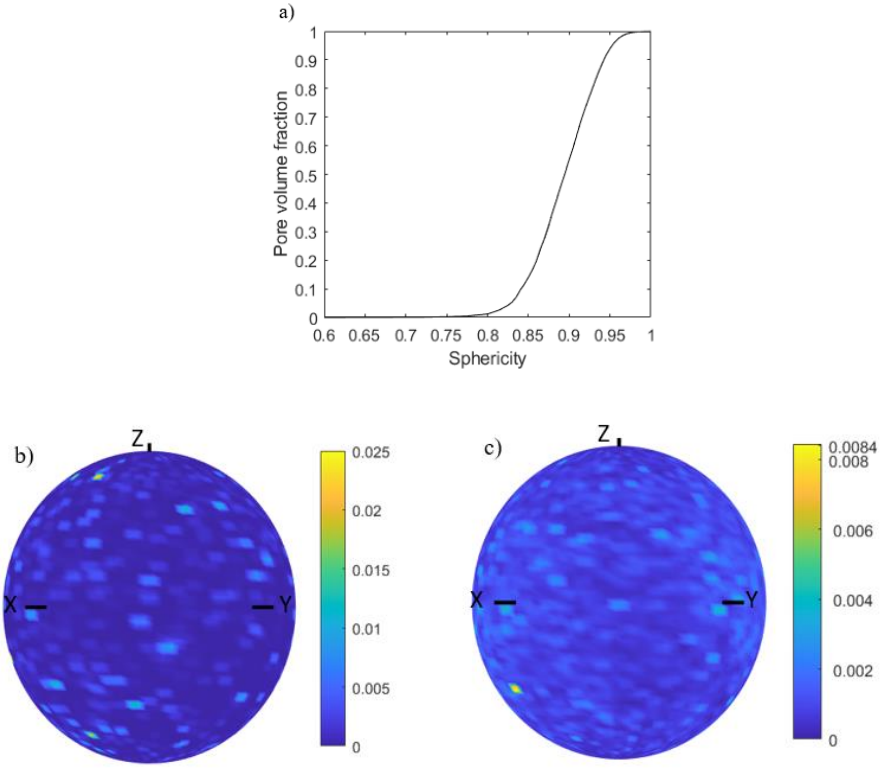

Fig. 2. a) Cumulative distribution of pore sphericity, b) orientation distribution of pores having sphericity $0.75<\psi<0.85$ and c) orientation distribution of pores having sphericity $0.85<\psi<0.95$

Orientation of each pore is calculated by approximating the pore as an equivalent ellipsoid using principal component analysis [9]. This is done using the 'regionprops3' function in MATLAB R2019b [10]. Spherical angles are then calculated for each pore from the eigenvectors obtained from the above MATLAB function. An orientation distribution function is plotted in the form of a spherical plot so that the distribution of pore orientations with respect to coordinate axes can be visualized. The pores are segregated into two sets, one which have sphericity in the range of 0.75 to 0.85 and other which have sphericity in the range of 0.85 to 0.95. Figs.2b and 2c show the orientation distribution of these pores respectively with the colormap showing pore volume fraction for each orientation.

3 Microstructure Studies Using Statistical Functions

In the theory of modelling random media, a wide variety of statistical functions have been used to define the distribution of phases within the heterogeneous medium [5]. This section describes five such functions that are employed in this article.

3.1 Two-point Correlation Function

Consider a n-dimensional 2 phase microstructure in which phase *i* occupies volume fraction v_i . An indicator function is defined such that:

$$I^{(i)}(\boldsymbol{x}) = \begin{cases} 1, & \boldsymbol{x} \in V_i \\ 0, & \text{otherwise} \end{cases} \tag{2}$$

where, V_i is the region occupied by the phase *i*. The two-point correlation function is defined as:

$$S_2^{(i)}(\boldsymbol{x_1}, \boldsymbol{x_2}) = \langle I^{(i)}(\boldsymbol{x_1})\, I^{(i)}(\boldsymbol{x_2}) \rangle. \tag{3}$$

It is defined as the probability of finding two points at positions $\boldsymbol{x_1}$ and $\boldsymbol{x_2}$ in the same phase in the medium. The brackets indicate ensemble average. For statistically homogeneous and isotropic medium, the two-point correlation function depends only on the magnitude of the distance between the two positions $r = |\boldsymbol{x_1} - \boldsymbol{x_2}|$. Hence it can be expressed in the form $S_2(r)$. This function gives an indication of the distribution of the phase within the medium.

3.2 Two-point Cluster Correlation Function

It is defined as the probability of finding two points at positions $\boldsymbol{x_1}$ and $\boldsymbol{x_2}$ in the same cluster (region of connected voxels of the same color) of the phase of interest in the medium. For statistically homogeneous and isotropic medium, this function depends only on the magnitude of the distance between the two positions $r = |\boldsymbol{x_1} - \boldsymbol{x_2}|$. Hence it can be expressed in the form $C_2(r)$. This function is a superior descriptor in the sense that it gives an idea of the connectedness of the phase of interest [11].

3.3 Lineal Path Function

It is defined as the probability of finding a line segment spanning from $\boldsymbol{x_1}$ to $\boldsymbol{x_2}$ that lies entirely in the phase of interest. The function contains some connectedness information along the lineal path (length of the segment) and hence contains certain long-range information about the medium. For statistically homogeneous and isotropic medium, the lineal path function depends only on the magnitude of the distance between the two positions $r = |\boldsymbol{x_1} - \boldsymbol{x_2}|$. Hence it can be expressed in the form $L(r)$.

3.4 Pore Size Distribution Function

The pore size distribution function, $P(\delta)$ is defined in such a way that $P(\delta)d\delta$ is the probability that a randomly chosen point in the pore phase (any phase of interest) lies at a distance between δ and $\delta + d\delta$ of the nearest point on the pore-solid interface. This function contains connectedness information about spherical regions in the pore phase. It can only be obtained from 3D images of the medium.

3.5 Cumulative Pore Size Distribution Function

It is defined as the probability $F(\delta)$ of the sphere of radius δ having its centre in the pore phase lie entirely in the pore phase. It is the fraction of the pore space that has pore diameter greater than δ.

Along with these functions, two one-point correlation functions called volume fraction and percolation volume fraction are also used in this article. Pore regions can either be connected or disconnected to each other. The fraction of the pore phase that percolates (connects) over the total volume of the phase in the medium is termed as percolation volume fraction. It is defined as ratio of the volume of largest cluster of connected pores to that of entire pore volume present in the medium.

For isotropic medium, it is sufficient to calculate $S_2(r)$, $C_2(r)$ and $L(r)$, only in the orthogonal directions [4]. This reduces the computational costs drastically as compared to brute force method in which these functions are calculated at all voxel positions and in all directions within the sample. Pore size distribution function can be directly evaluated by calculating the Euclidean distance transform of a binary 3D image. The result gives a 3D matrix in which each element is the distance between that voxel and the nearest nonzero voxel (or voxel from different phase) in the binary image. This matrix can be used to bin the voxels based upon the value they possess. The number of voxels in each bin is normalized by the total number of voxels in the phase of interest. A graph of these values with respect to corresponding bin value of δ is plotted. For calculating cumulative pore size distribution function, the transformed matrix obtained while determining the pore size distribution function is used and the unique values of δ are determined and stored in a column vector. Then at each position of the transformed matrix, all the values lower than its value in that position are selected. Then counters corresponding to each of those values are increased. This process is repeated at each voxel element of the transformed matrix. Finally, the values of each counter are normalized by the total number of voxels in the phase of interest. A graph of these values

with respect to the corresponding value of δ is plotted. To calculate percolation volume fraction, the volume of each cluster determined while finding two-point cluster correlation function is calculated and divided by the total volume of the phase of interest. The maximum of these volume fractions is the percolation volume fraction.

For selected foam sample, all these functions are calculated using above described methods to study distribution of pore phase. Note that from here onwards the binary image before segmentation is used. The results are given in Figs. 3a-3e and Table.1.

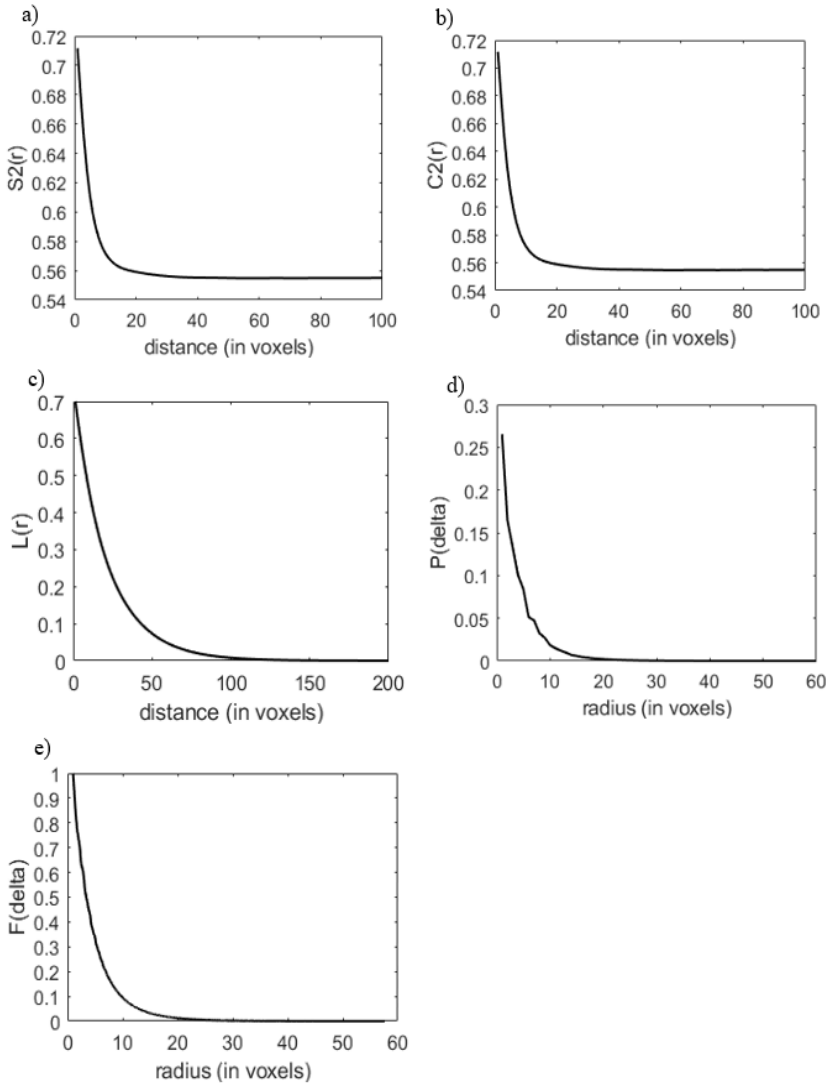

Fig. 3. a) Two-point correlation function; b) Two-point cluster correlation function; c) Lineal path function; d) Pore size distribution function; e) Cumulative pore size distribution function of the alumina foam sample.

Table 1. One-point correlation functions

Volume fraction v	0.745
Percolation volume fraction v^*	0.999

It is observed that for the selected microstructure, since the percolation volume fraction is close to 1, there is no difference between two-point correlation function and two-point cluster correlation function. Hence in the remainder of the article, cluster correlation function will not be used for studying the microstructure. Similarly, it is decided not to use pore size distribution function as cumulative pore size distribution function is smoother and contains all the required information about the pore phase that will be needed further. In order to check the isotropy of the foam sample, the functions $S_2(r)$ and $L(r)$ are calculated individually for each orthogonal direction and plotted to check if these functions vary in different directions. The results are given in Figs. 4a-4b.

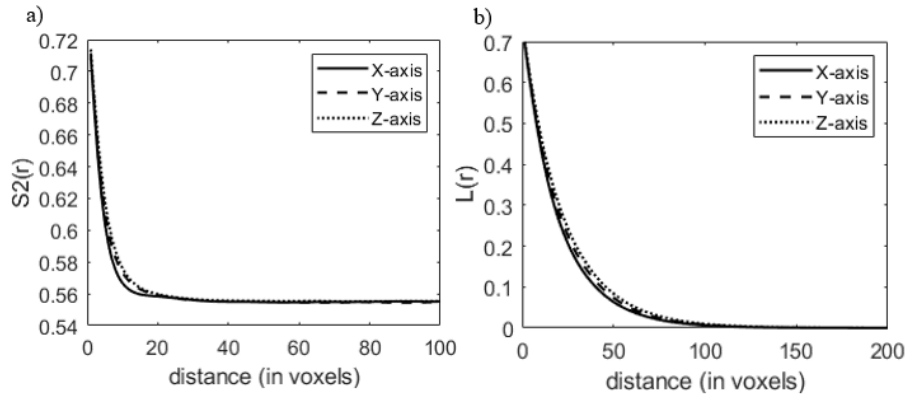

Fig. 4. a) Two-point correlation function and b) Lineal path function in three orthogonal directions

4 Selection of SVE Size

The foam sample under question is too big to be used directly for finite element (FE) calculations. Hence appropriate size and position within the sample is to be chosen for further use in FE calculations. Since the material microstructure is random in nature, an ensemble of stochastic volume elements is to be found. For this purpose, the foam sample is divided into smaller regions and statistical functions for realizations of each size are calculated. Fig. 5 shows different sizes considered in this study. Note that each volume element (VE) is cuboidal in shape. For ease of representation it is shown in two dimensions.

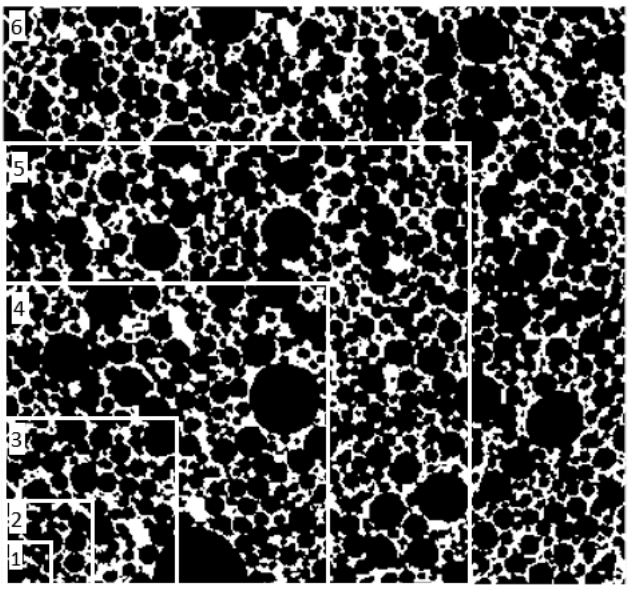

Fig. 5. Different sizes of VEs

Table 2. Dimension and number of realizations of each VE size

VE Size	Relative edge length	No. of realizations
1	1/16	4096
2	1/8	512
3	1/4	64
4	1/2	8
5	3/4	8
6	1	1

Edge length of each VE size in terms of edge length of the entire sample (size 6) is given in Table.2. Realizations for sizes 1 ,2, 3 and 4 are formed by shifting the VE domain one edge length at a time in all three directions. Realizations for size 5 are formed by considering 2 realizations in each direction such that all the sample space is utilized. Since the VEs are stochastic, the number of VEs in ensemble of each size plays a critical role in determining any useful conclusions from the VEs. The Figs. 6a-6d show the effect of number of samples in the ensemble of each VE size on averaged statistical functions. Here Euclidean norm of each statistical function for each VE is calculated. Since sample size (number of realizations) in ensemble of each VE size is different, the sample size plotted on X-axis is normalized with respect to the total number of realizations for each VE size. Figs.7a-7d show scatter of norms of statistical functions for each VE size. The solid line indicates mean value for each VE size.

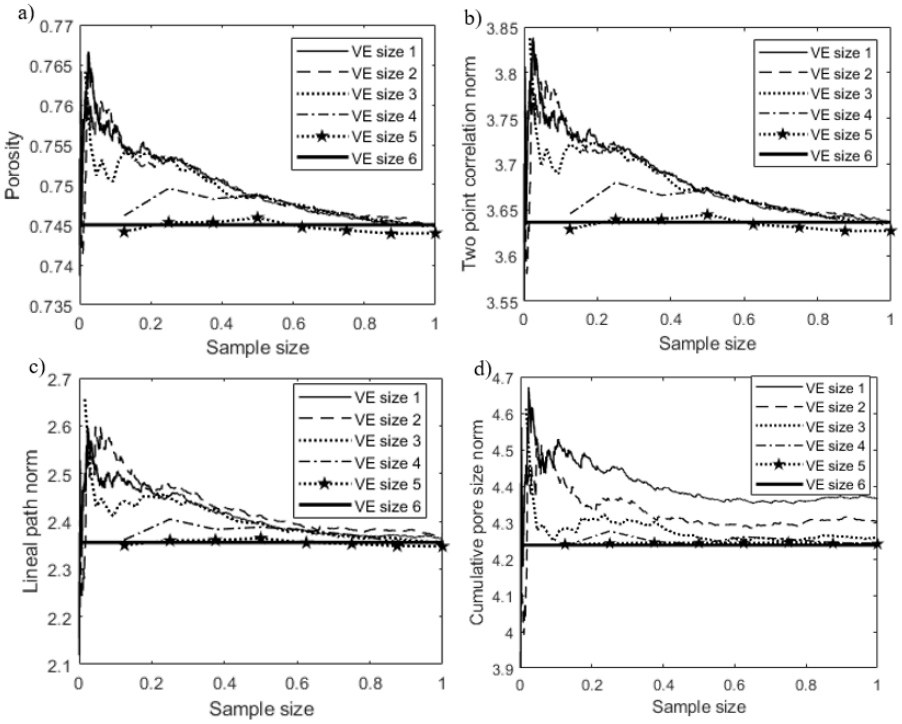

Fig. 6. Effect of sample size on a) porosity; norm of b) two-point correlation function; c) lineal path function and d) cumulative pore size distribution function for each VE size

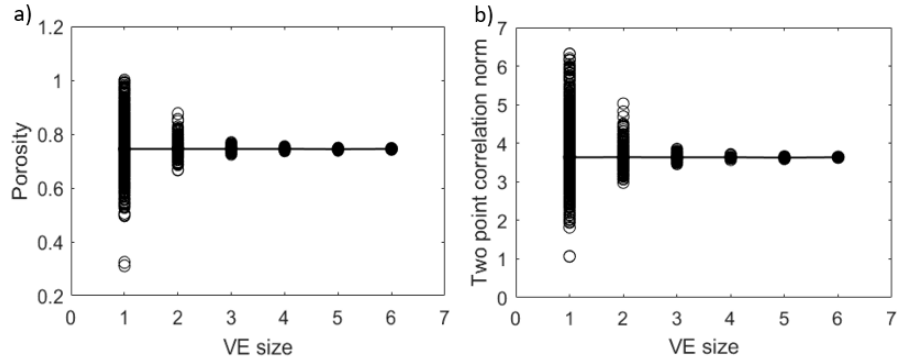

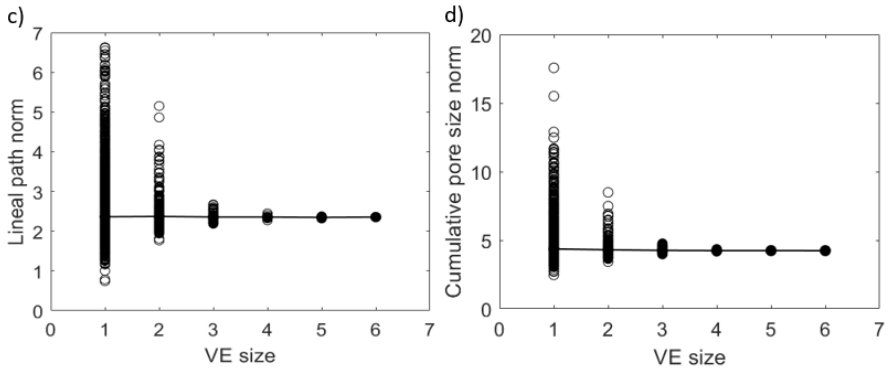

Fig. 7. Scatter of a) porosity; norm of b) two-point correlation function; c) lineal path function and d) cumulative pore size distribution function for each VE size along with their average values

It can be seen from Figs.6a-6c that for each VE size, the ensemble average approaches the value of the entire sample (size 6) when all the realizations are taken into account. Since the number of realizations increase as VE size decreases, a greater number of realizations are needed in the ensemble average to reach the value of entire sample as the VE size is decreased. Fig. 6d shows that the ensemble average of cumulative pore size norm approaches that of the entire sample for size 3 and above. The scatter in the results of each VE size is shown in Figs. 7a-7d. Mean value of each VE size equals the value of the entire sample after utilizing all the realizations in each ensemble. Hence choice of appropriate VE size for FE calculations depends upon the size of VE that can be handled by the available computational resources and the number of realizations. For further studies in this article, VEs of size 3 are taken as stochastic volume elements (SVEs). It is because, for this size, the ensemble average of all the four statistical functions converge to that of the entire sample (Figs.6a-6d) and it gave results with acceptable computational expenses.

5 Ranking of SVEs

In the previous section, it was decided to use VE size 3 as SVE in further calculations of effective elastic properties. A straight forward way to do this is to calculate effective properties of all the realizations in the ensemble of size 3 and then calculate ensemble average of the effective properties. However, this would need significant computational expenses. Statistical functions can be used here to reduce the number of realizations used in the ensemble averaging. Here, absolute value norm of the percentage difference between statistical functions of each SVE in the ensemble and that of the entire foam sample is calculated. For each SVE, functions $S_2(r)$, $L(r)$, $F(\delta)$ and volume fraction are evaluated. These results are then rearranged in ascending order of SVEs and plotted in Figs. 8a-8d.

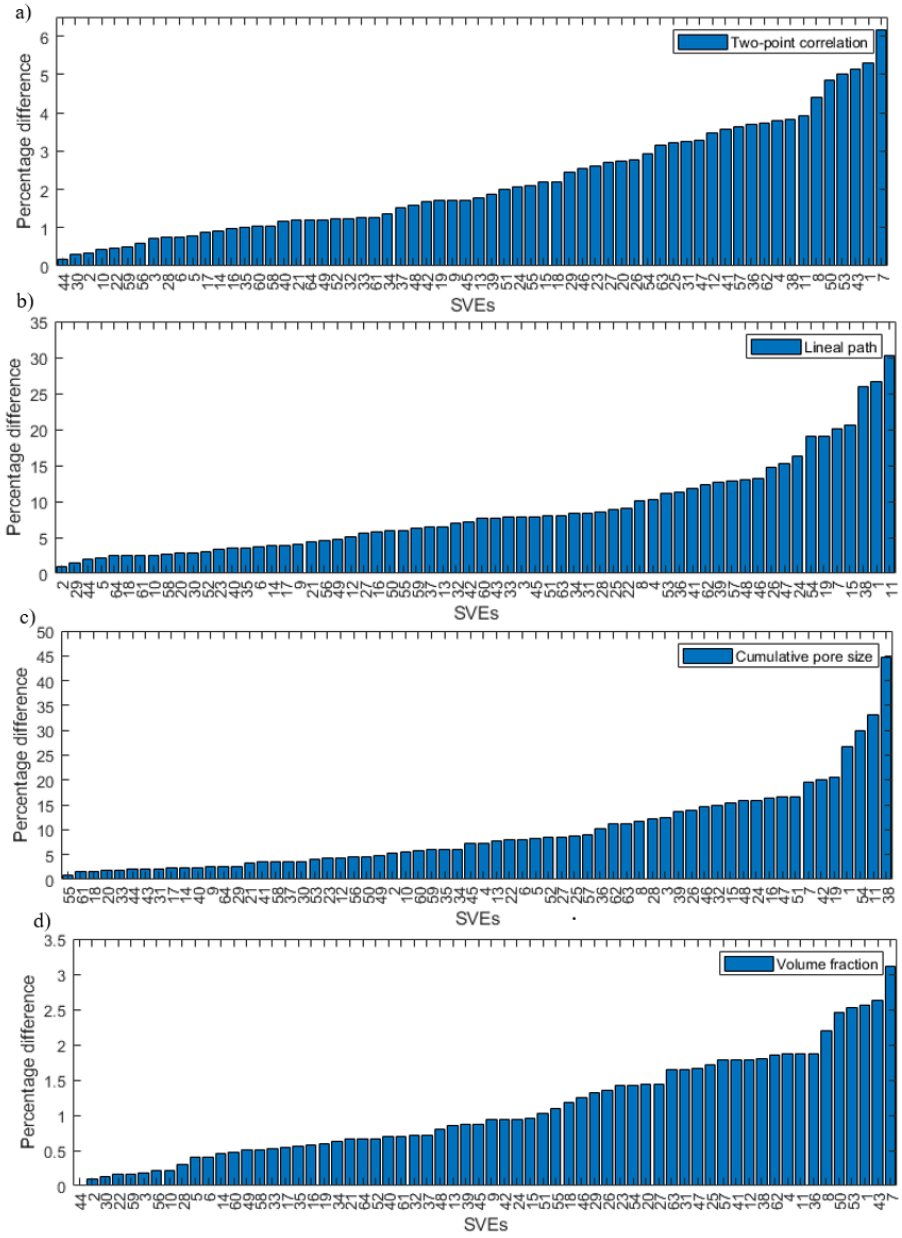

Fig. 8. Ranking of SVEs for a) two-point correlation function; b) lineal path function; c) cumulative pore size distribution function and d) porosity (pore volume fraction)

It can be seen that for each statistical function, the ranking of SVEs varies. Hence it is decided to use the SVEs that lie within 5% value for all statistical functions. 5 SVEs are obtained that satisfied this criterion. They are SVE no. 14, 17, 30, 44 and 58. Hence,

instead of using all 64 realizations of the SVEs, these 5 SVEs are selected for ensemble averaging of effective elastic properties.

6 Determination of Effective Elastic Properties

The problem of determination of effective properties is based upon the idea that a heterogeneous medium can be converted into a homogeneous medium by utilizing the conservation of energy principle. The criteria given by Hill [12] needs to be satisfied:

$$\langle \boldsymbol{\sigma} : \boldsymbol{\varepsilon} \rangle = \langle \boldsymbol{\sigma} \rangle : \langle \boldsymbol{\varepsilon} \rangle . \tag{4}$$

It says that average of the scalar product of stress $\boldsymbol{\sigma}$ and strain $\boldsymbol{\varepsilon}$ tensors over the heterogeneous medium should be equal to the product of their individual averages. Using Gauss theorem, this condition can be generalized for heterogeneous materials [6] as:

$$\int_{\Gamma} (\boldsymbol{t}(\boldsymbol{x}) - \langle \boldsymbol{\sigma} \rangle \cdot \boldsymbol{n}) \cdot (\boldsymbol{u}(\boldsymbol{x}) - \langle \boldsymbol{\varepsilon} \rangle \cdot \boldsymbol{x}) \, d\Gamma = 0 . \tag{5}$$

Where Γ is boundary of a VE and $\boldsymbol{t}$, $\boldsymbol{n}$, $\boldsymbol{u}$ and $\boldsymbol{x}$ are the traction, normal, displacement and position vectors respectively. This condition is satisfied by three types of boundary conditions [13, 14] namely kinematic uniform boundary condition (KUBC), stress uniform boundary condition (SUBC) and mixed uniform boundary condition (MUBC). [15] showed that KUBCs and SUBCs give bounds to the apparent stiffness tensor ($\mathbf{C}$):

$$\boldsymbol{C}_{SUBC} \leq \boldsymbol{C}_{MUBC} \leq \boldsymbol{C}_{KUBC} . \tag{6}$$

Also,

$$\boldsymbol{C}_{SUBC} \leq \boldsymbol{C}_{eff} \leq \boldsymbol{C}_{KUBC} . \tag{7}$$

Where, $\boldsymbol{C}_{eff}$ is the exact effective stiffness tensor of the heterogeneous medium. Using the fact that periodic boundary conditions (PBCs) give exact effective stiffness tensor of periodic microstructures, [6] showed that the periodically compatible mixed boundary conditions (PMUBCs) give effective stiffness tensor for non-periodic microstructures that match closely with that obtained by applying PBCs on the same sample by converting it into periodic. This conversion was done by mirroring the non – periodic sample about its three orthogonal planes. These PMUBCs are utilized in this article so as to obtain effective stiffness tensor of the five selected SVEs.

The SVE problem is defined as:

$$div(\boldsymbol{\sigma}) = 0 \text{ in } \Gamma. \tag{8}$$

Such that the boundary conditions satisfy:

$$\langle \boldsymbol{\sigma} : \boldsymbol{\varepsilon} \rangle = \langle \boldsymbol{\sigma} \rangle : \langle \boldsymbol{\varepsilon} \rangle . \tag{9}$$

The coordinate system, dimensions and nomenclature of faces of Γ are given in Fig.9.

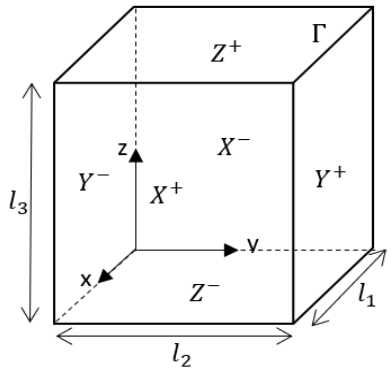

Fig. 9. Representation of Γ

The problem is solved numerically by using finite element method. A commercial software called ABAQUS [16] is used for this purpose. Each SVE sample is meshed using linear tetrahedral elements such that the alumina phase is meshed and the pore phase is kept unmeshed. The elastic material properties of alumina [3] were taken as E=360.5GPa and ν = 0.2. The effective stiffness tensor **C** is expressed as:

$$\boldsymbol{\sigma} = \boldsymbol{C} : \boldsymbol{\varepsilon} \,. \tag{10}$$

Writing in terms of the respective components, taking into account the symmetries of the tensors and using Voigt notation:

$$\begin{bmatrix} \sigma_{11} \\ \sigma_{22} \\ \sigma_{33} \\ \sigma_{12} \\ \sigma_{23} \\ \sigma_{31} \end{bmatrix} = \begin{bmatrix} C_{11} & C_{12} & C_{13} & C_{14} & C_{15} & C_{16} \\ C_{21} & C_{22} & C_{23} & C_{24} & C_{25} & C_{26} \\ C_{31} & C_{32} & C_{33} & C_{34} & C_{35} & C_{36} \\ C_{41} & C_{42} & C_{43} & C_{44} & C_{45} & C_{46} \\ C_{51} & C_{52} & C_{53} & C_{54} & C_{55} & C_{56} \\ C_{61} & C_{62} & C_{63} & C_{64} & C_{65} & C_{66} \end{bmatrix} \begin{bmatrix} \varepsilon_{11} \\ \varepsilon_{22} \\ \varepsilon_{33} \\ 2\varepsilon_{12} \\ 2\varepsilon_{23} \\ 2\varepsilon_{31} \end{bmatrix} \tag{11}$$

PMUBCs are given in Table.3. Note that 1→x, 2→y and 3→z in the description of boundary conditions. In the FE simulations, six load cases are defined. In each load case, one strain component with value 0.001 is applied according to Table.3. The corresponding stress tensor is calculated as average stress over the SVE using:

$$\langle \boldsymbol{\sigma} \rangle = \frac{1}{V_\Gamma} \int_\Gamma \boldsymbol{\sigma}(\boldsymbol{x}) d\Gamma(\boldsymbol{x}) \,. \tag{12}$$

From the results of each load case, each column of stiffness tensor is calculated. FE mesh of SVE 14 is shown in Fig. 10. To apply boundary conditions, all the nodes that lie on each face of the SVE are selected and their degrees of freedom are constrained according to Table.3. The results of the FE simulations are given in Table.4. The unit of stiffness coefficients is GPa. It also contains the results of experimental measurements of the same material referred from [3].

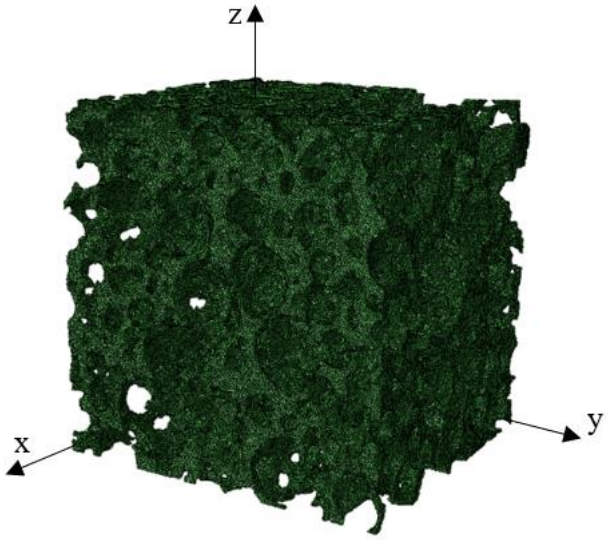

Fig. 10. Finite element mesh of SVE 14

Table 3. PMUBCs on each face of SVE for six load cases

	$X^{\pm}$	$Y^{\pm}$	$Z^{\pm}$
Tension X	$u_1 = \pm\varepsilon_{11}^0 \frac{l_1}{2}$ $t_2 = t_3 = 0$	$u_2 = 0$ $t_1 = t_3 = 0$	$u_3 = 0$ $t_1 = t_2 = 0$
Tension Y	$u_1 = 0$ $t_2 = t_3 = 0$	$u_2 = \pm\varepsilon_{22}^0 \frac{l_2}{2}$ $t_1 = t_3 = 0$	$u_3 = 0$ $t_1 = t_2 = 0$
Tension Z	$u_1 = 0$ $t_2 = t_3 = 0$	$u_2 = 0$ $t_1 = t_3 = 0$	$u_3 = \pm\varepsilon_{33}^0 \frac{l_3}{2}$ $t_1 = t_2 = 0$
Shear XY	$u_2 = \pm\varepsilon_{21}^0 \frac{l_1}{2}$ $u_3 = t_1 = 0$	$u_1 = \pm\varepsilon_{12}^0 \frac{l_2}{2}$ $u_3 = t_1 = 0$	$u_3 = 0$ $t_1 = t_2 = 0$
Shear YZ	$u_1 = 0$ $t_2 = t_3 = 0$	$u_3 = \pm\varepsilon_{32}^0 \frac{l_2}{2}$ $u_1 = t_2 = 0$	$u_2 = \pm\varepsilon_{23}^0 \frac{l_3}{2}$ $u_1 = t_3 = 0$
Shear ZX	$u_3 = \pm\varepsilon_{31}^0 \frac{l_1}{2}$ $u_2 = t_1 = 0$	$u_2 = 0$ $t_1 = t_3 = 0$	$u_1 = \pm\varepsilon_{13}^0 \frac{l_3}{2}$ $u_2 = t_3 = 0$

Table 4. Stiffness coefficients (in GPa) for 5 SVEs and experimental results

	C_{11}	C_{22}	C_{33}	C_{44}	C_{55}	C_{66}	Porosity (%)
SVE 14	19.58	22.87	27.96	6.79	8.63	7.64	74.8
SVE 17	23.71	26.59	29.47	8.01	9.23	8.84	74.9
SVE 30	22.94	28.09	31.53	8.28	9.84	9.06	74.4
SVE 44	25.15	26.11	28.65	8.83	8.92	9.06	74.5
SVE 58	26.37	29.33	29.62	9.25	9.99	9.29	74.1
SVE Average	23.55	26.60	29.45	8.23	9.32	8.78	74.5
Average	26.54			8.78			
Experiments [3]	30.2	29.8	28.5	7.2	6.7	N. A	74.5
Average	29.5			6.95			

7 Discussion

The article demonstrates the use of statistical functions in characterizing the microstructure of alumina foam which acts as a preform for manufacturing interpenetrating phase composites. A detailed explanation of image processing steps used to convert the grey-scale CT scans into 3D binary image of foam sample has been given. The image is segmented to isolate the interconnected pores so that each pore could be studied. It is observed in Fig.2a that all the pores have more than 0.75 sphericity which indicates that the pores resemble closely to spheres. This is an indication of isotropy of the microstructure. Figs. 2b-2c show that the pores do not have any preferential orientation. Fig.2b has two bright yellow spots close to Z axis and Fig.2c has one bright yellow spot close to X axis. However, their volume fractions are very less and hence will not impact the effective properties of the sample in any way.

Fig 3 shows statistical functions of the entire foam sample. Only for statistically homogeneous microstructure without long-rang order, $S_2(r)$ follows limits:

$$S_2(r=0) = v\,, \tag{13}$$

$$\lim_{r\to\infty} S_2(r) = v^2\,. \tag{14}$$

Here, v is the volume fraction of pores. In our case, $\lim_{r\to 0} S_2(r) = 0.72$ and $\lim_{r\to\infty} S_2(r) = 0.55$. Hence, the limits are satisfied. This proves that the sample is highly homogeneous. Note that the value of $S_2(r)$ at $r = 0$ does not exactly match value of volume fraction (refer Table.1) because of the limitations in image resolutions. Improved resolutions can bring this value closer to the volume fraction. $S_2(r)$ also becomes asymptotic above 35 voxels distance. It means that above this value, there is no observable correlation in the pore voxels. The lineal path function (Fig.3c) becomes asymptotic at around 100 voxels distance. This means that the interconnectedness along lineal path is observable only till the distance of 100 voxels. The cumulative pore size

distribution function (Fig.3e) shows that the maximum radius of the spherical pore that can be fitted into the pore space is around 25 voxels. Fig. 4 shows that $S_2(r)$ and $L(r)$ have almost same curves when calculated along three orthogonal directions. This proves that the sample is isotropic as well.

Figs. 6a-6d show the effect of number of realizations on ensemble average values of statistical functions. It can be seen that as the VE size decreases, the number of realizations in the ensemble required to match the value of the entire sample increases. Hence, while choosing the appropriate size of VE, a trade-off is required between VE size and number of realizations. In case of VE size 5, the ensemble average lies very close to that of the entire sample irrespective of number of realizations considered in averaging. This is because the difference between this size and that of the entire sample is very less. The fluctuations in the curves are probably because all the 8 VEs in this ensemble share a lot of common region. Hence not enough independent realizations are available to get converging results. Figs.7a-7d show that if enough number of realizations are considered, the ensemble average of statistical functions matches the value of that of the entire sample. As explained before, the choice of VE size for FE calculations depend upon the available computational resources. The VE size 3 chosen in this study satisfies the requirements to be SVE and also fits the computational resources available.

In order to reduce the computational expense of doing FE calculations on 64 realizations of VE size 3, a ranking method is developed. Here, the difference between the statistical functions of each realization and that of the entire sample is calculated and the SVEs are ranked in ascending order of these values (Figs. 8a-8d). Each statistical function has a different ranking order. Hence, it is decided to find those SVEs that lie within 5 % value for all statistical functions. Since these SVEs have microstructure that resemble the most to that of the entire sample, it is decided to perform ensemble averaging on only these 5 SVEs as against 64 SVEs that would have otherwise required. This has significantly reduced the required computational expenses.

Results of FE calculations are given in Table.4 which shows the diagonal coefficients of effective stiffness tensor for all 5 SVEs. Averaging across all SVEs gives us the SVE averages. We can conclude from these values that the foam sample can be considered as isotropic. The experimental results [3] along the three directions also support this statement. Note that the average porosity of the SVEs matches that of the experimental results. Considering isotropy, average of SVE averages C_{11}, C_{22} and C_{33} gives value of 26.5 GPa. Similarly, averaging of experimental results [3] of C_{11}, C_{22} and C_{33} gives value of 29.5 GPa. The simulated value is within 10% deviation of the experimental value. Repeating this for SVE averages C_{44} , C_{55} and C_{66} gives value of 8.78 GPa and for experimental results [3], value of 6.95 GPa. The simulated value is within 20% deviation of the experimental value. These values prove that the adopted procedure of selecting SVE size, ranking method and the numerical calculations predict the effective elastic properties of ceramic foam with a very high degree of accuracy. Further reduction in this deviation can be achieved by using better resolution of CT scan images.

8 Conclusions

This article describes the use of statistical functions to characterize the microstructure of ceramic foam and to use these functions to select appropriate size, number and location of SVEs that are further used for determining effective elastic properties of the foam sample. This has led to reduction in size and number of realizations required to determine effective properties of the material which otherwise would have required significant computational resources. The article also demonstrates the suitability of using PMUBCs to determine the effective material properties of non-periodic microstructures with phases having extreme contrast in material properties (infinity in this case).

The larger goal of this research is to establish structure-property-performance relationship links for the ceramic foam material. The statistical functions act as a tool to quantify the microstructure. An important part of this research is to establish a correlation between the statistical functions and the mechanical properties of this material. This will act as a guide in an inverse problem of identifying appropriate microstructure for target material properties. As per authors knowledge, such method does not exist for a microstructure that is unique to foams. In this paper as a first step, an attempt has been made to determine effective elastic properties of foam by using the statistical functions to reduce the ensemble size.

In existing literature, only the effect of volume fraction on the elastic properties has been studied so far. The next step in this research is to artificially reconstruct the microstructure using target correlation functions and then change each statistical function to study its effect on material elastic properties. This way each function can be controlled precisely. This will be followed by sensitivity analysis of each statistical function w.r.t effective material properties. Correlations between the statistical functions if any will be studied as well. Currently this cannot be done as the microstructure that has been used was derived from X-ray computed tomography and hence there was no control over the statistical functions. Once these steps are done, the research will shift its focus on predicting appropriate microstructures for performance enhancement of the material.

Acknowledgements

The financial support of the Darmstadt University of Applied Sciences is gratefully acknowledged. The publication partially uses raw and experimental data provided by the project WE 4273/17-1 funded by the DFG. Their financial support is gratefully acknowledged. In this regard, special thanks go to Joél Schukraft for the experimental support. The authors thank Morgan Advanced Materials Haldenwanger GmbH for the friendly supply of complimentary ceramic foam material.

References

1. Chawla, K. K. Composite materials, Springer, New York (2012). DOI:10.1007/978-0-387-74365-3
2. Wegner, L. D., & Gibson, L. J. The mechanical behaviour of interpenetrating phase composites–I: modelling. International Journal of Mechanical Sciences, 42(5), 925-942 (2000). DOI:10.1016/S0020-7403(99)00025-9
3. Horny, D. et al. Numerical and experimental characterization of elastic properties of a novel, highly homogeneous interpenetrating metal ceramic composite. Advanced Engineering Materials, 1901556 (2020). DOI:10.1002/adem.201901556
4. Torquato, S. Random Heterogeneous Materials: Microstructure and Macroscopic Properties, Springer, New York (2002). DOI:10.1007/978-1-4757-6355-3
5. Torquato, S. Optimal design of heterogeneous materials. Annual review of materials research, 40, 101-129 (2010). DOI:10.1146/annurev-matsci-070909-104517
6. Pahr, D. H., & Zysset, P. K. Influence of boundary conditions on computed apparent elastic properties of cancellous bone. Biomechanics and modeling in mechanobiology, 7(6), 463-476 (2008). DOI:10.1007/s10237-007-0109-7
7. Meyer, F. Topographic distance and watershed lines. Signal processing, 38(1), 113-125 (1994). DOI:10.1016/0165-1684(94)90060-4
8. Wang, D., & Fan, L. S. Particle characterization and behavior relevant to fluidized bed combustion and gasification systems. In Fluidized bed technologies for near-zero emission combustion and gasification (pp. 42-76). Woodhead Publishing (2013). DOI: 10.1533/9780857098801.1.42
9. Drach, B., Tsukrov, I., Gross, T., Dietrich, S., Weidenmann, K., Piat, R., & Böhlke, T. Numerical modeling of carbon/carbon composites with nanotextured matrix and 3D pores of irregular shapes. International Journal of Solids and Structures, 48(18), 2447-2457 (2011). DOI:10.1016/j.ijsolstr.2011.04.021
10. Matlab R2019b. https://de.mathworks.com/products/new_products/release2019b.html
11. Jiao, Y., Stillinger, F. H., & Torquato, S. A superior descriptor of random textures and its predictive capacity. Proceedings of the National Academy of Sciences, 106(42), 17634-17639 (2009). DOI:10.1073/pnas.0905919106
12. Hill, R. Elastic properties of reinforced solids: some theoretical principles. Journal of the Mechanics and Physics of Solids, 11(5), 357-372 (1963). DOI:10.1016/0022-5096(63)90036-X
13. Hazanov, S., & Amieur, M. On overall properties of elastic heterogeneous bodies smaller than the representative volume. International Journal of Engineering Science, 33(9), 1289-1301 (1995). DOI:10.1016/0020-7225(94)00129-8
14. Ostoja-Starzewski, M. Material spatial randomness: From statistical to representative volume element. Probabilistic engineering mechanics, 21(2), 112-132 (2006). DOI:10.1016/j.probengmech.2005.07.007
15. Hazanov, S., & Huet, C. Order relationships for boundary conditions effect in heterogeneous bodies smaller than the representative volume. Journal of the Mechanics and Physics of Solids, 42(12), 1995-2011 (1994). DOI:10.1016/0022-5096(94)90022-1
16. Abaqus, Simulia. https://www.3ds.com/products-services/simulia/products/abaqus/